CHAPTER 5 *Braided Composite Frame Tests*

The static test results are presented and discussed for braided composite frame B in Section 5.1, and for frame C in Section 5.2. Results from the numerical analysis of these frames using the ABAQUS computer code are presented in Section 5.3.

5.1 Test results of braided composite frame B

The load-displacement curve from the test of frame B is shown in Fig. 5.1. In the initial portion of the response the load-displacement data plot is a straight line with a slope of 14887 lb/in, and at larger loads the slope of the data line decreases. The first major failure event occurs at the point labeled B_1 in the figure (5791.6 lb, 0.4782 in.), and then the force drops to 3475.3 lb at this displacement. At this first drop in the load, a crack initiates at the junction of the web and outer flange at the apex ($q = 0°$) and propagates through the upper half of the web (the portion of the web adjacent to the radially outboard flange). As the test continues, a reloading at a stiffness lower than the initial stiffness takes place. The second major failure event occurs at point B_2 (3878.7 lb, 0.6726 in.). At this second failure, the crack that developed in the upper part of the web at failure B_1 propagates to the lower part of the web (the portion closer to the radially inboard flange), completely fracturing the web at the apex of the frame (Fig. 5.2). There is another drop in the load and a subsequent reloading at a lower stiffness than before. The third major failure event occurs at point B_3

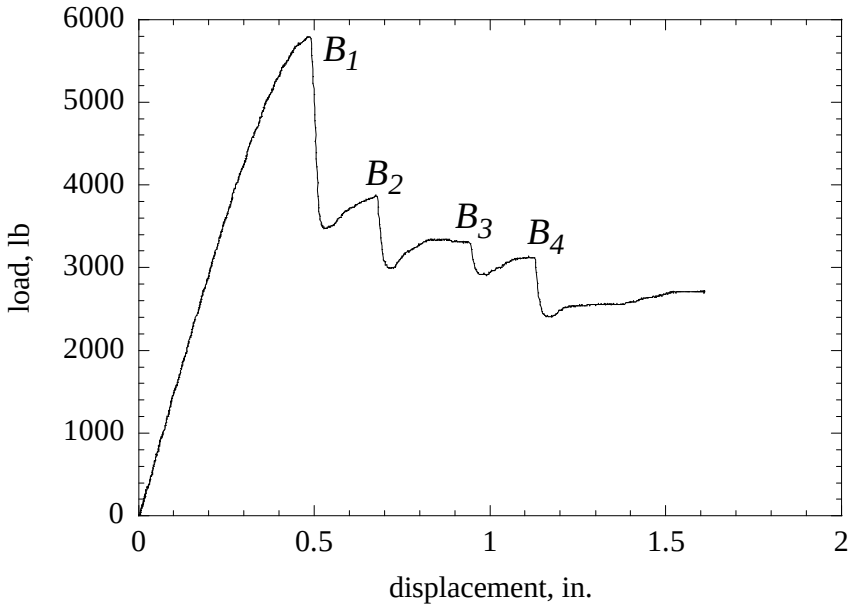

Fig. 5.1 Load-displacement data from the test of braided frame B.

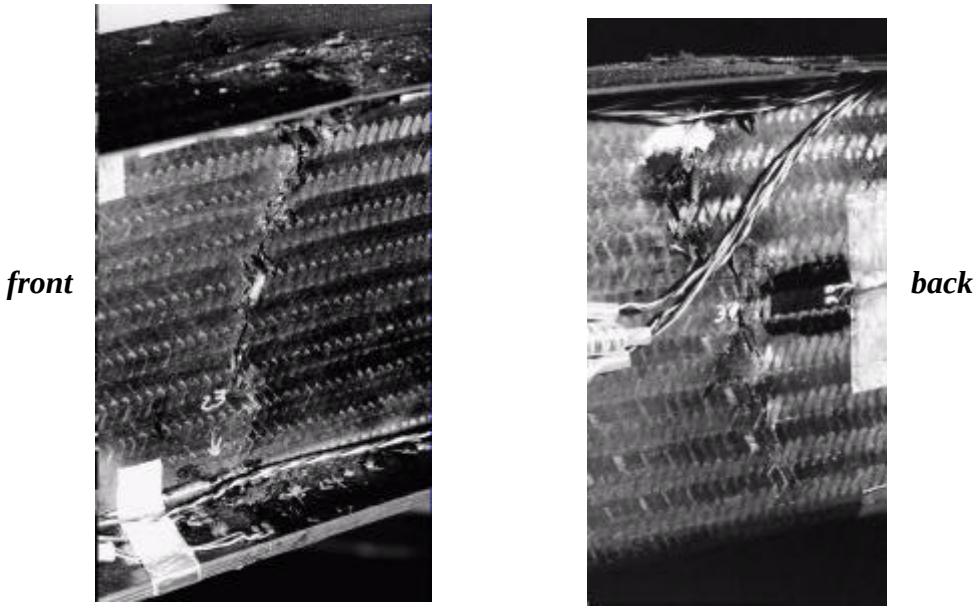

Fig. 5.2 Braided composite frame B after first failure event. The crack in the web is located at the apex of the frame.

(3319.2 lb, 0.9366 in.). The crack in the web at the apex of the frame propagates from the junction of the web and outer flange through one side of the outer flange. There is a drop

in the load at this third failure event, followed by a reloading to the fourth failure event at point B_4 (3124 lb, 1.125 in.), where a fourth drop in the load occurs. The crack at the apex propagates to the other side of the outer flange, completely fracturing the outer flange. After the force drop at point B_4, another reloading occurs. Only the inner flange remains intact at the apex of the frame. The test is stopped before the crack could propagate through the inner flange. The surface fractures tend to follow the ± 64° braider yarns in a zigzag pattern similar to what is observed in the tensile and flexure test coupons. After the test, some damage is also observed in the inner flange, at both ends of the frame.

The distribution of the circumferential strain data around frame B at different force levels is shown in Fig. 5.3 for the outer flange. The maximum compression strains in the

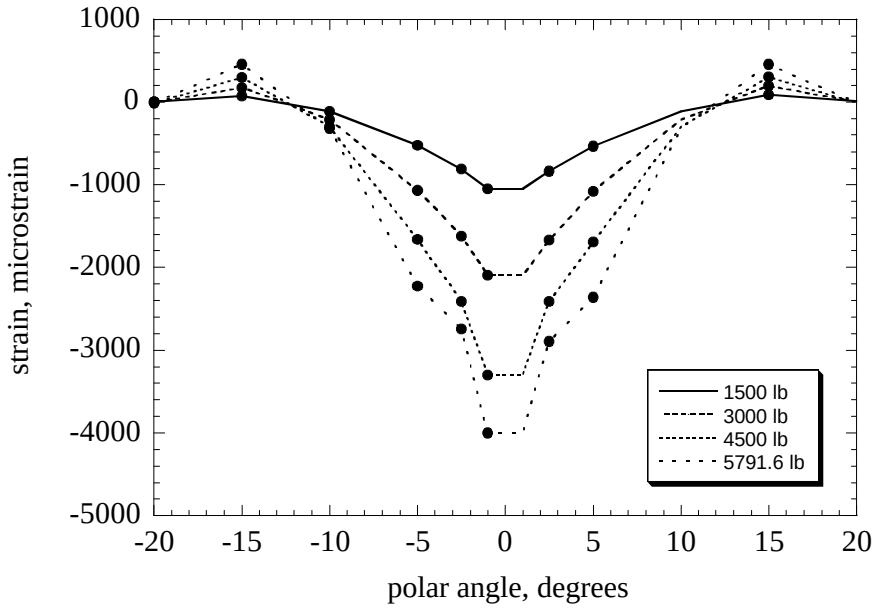

Fig. 5.3 Circumferential strain data in the outer flange from the test of frame B.

outer flange occur at the apex (q = 0°), and maximum tensile strains occur at about q = ± 15°; i.e., near both ends of frame B. The circumferential strain data around the inner flange at different force levels are shown in Fig. 5.4. Peak tensile strains occur in the inner flange at the apex (q = 0°), but the magnitude of this peak is lower than the compressive strain magnitudes occurring in the inner flange at the ends of the frame. The failures

occurring at the apex of the frame (q = 0°) in the outer flange, and at the ends of the frame in the inner flange, coincide with the highest circumferential strains registered throughout the test.

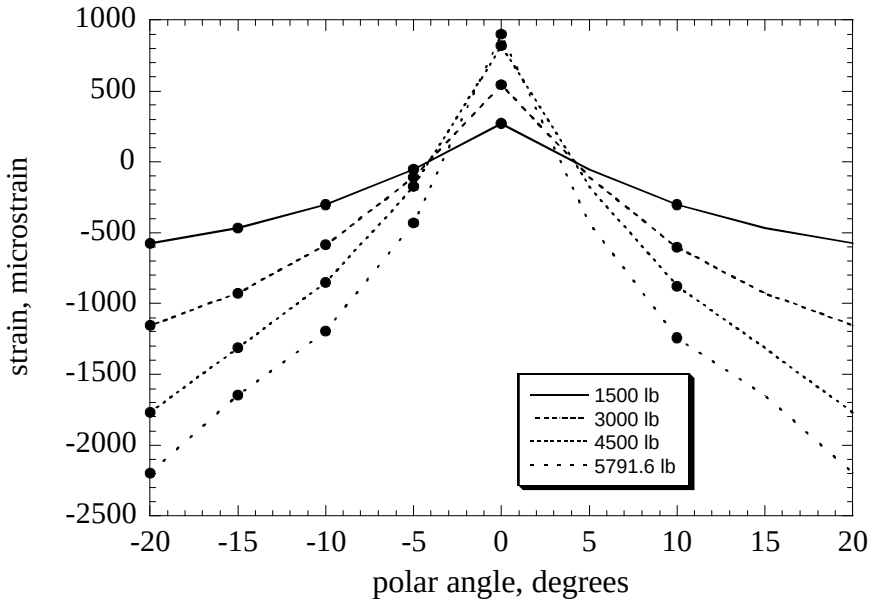

Fig. 5.4 Circumferential strain data in the inner flange from the test of frame B.

From the circumferential strain data on the inner and outer flanges, we can construct extensional and bending strain data around the circumference of frame B. The extensional strain is calculated as the sum of the circumferential strains in the outer flange and the inner flange at the same circumferential location and load divided by two. The bending strain is calculated as the difference between the circumferential strains of the outer flange and the inner flange at the same circumferential location and load divided by two. Presenting the circumferential strains as an extensional part and a bending part identifies the deformation components of the frame response as a one-dimensional structural member. The bending strain data for frame B are shown in Fig. 5.5. From this figure it is seen that the largest bending strain is at the apex (q = 0°) of frame B. Also there is an inflection point between eight and nine degrees which demarcates the point where the bending strain is changing sign. The extensional strain data is shown in Fig. 5.6. The extensional strains

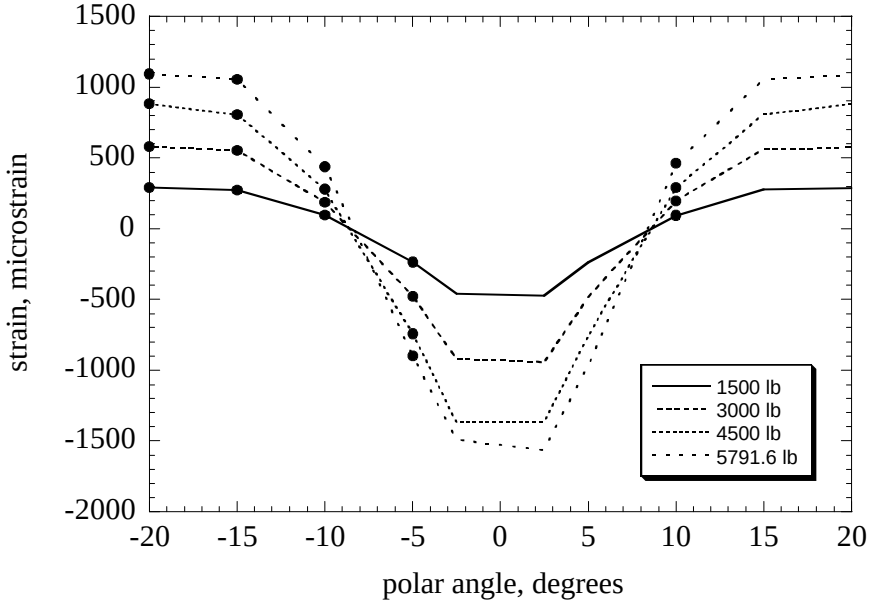

Fig. 5.5 Bending strain data from the test of frame B.

of the largest magnitude also occur at the center of the apex (q = 0°) for frame B, although high strains are also observed at both ends of the frame for each load level.

The few shear strain data obtained from the test of frame B are shown in Fig. 5.7. There are only four rosettes to measure the shear strains on one side of the web, and these are located at $q = \pm 2.5°$, and $q = \pm 15°$. Although the shear strain data is limited, the data shown in Fig. 5.7 can give some insight in the shear response of the frame. The shear strain data corresponding to the lower load levels show the expected anti-symmetric distribution of the shear strain about the apex of the frame. The only data that does not appear anti-symmetric are those corresponding to the failure load of 5791.6 lb.

As the displacement of the testing machine's table increased, the contact region at the apex of the frame between the platen and the outer flange increased. This contact tends to suppress the twist and out-of-plane displacement of the outer flange of the frame in contact with the platen. However, twist and out-of-plane displacement of the frame outside of the contact region is observed in the test. As will be shown from the test data of frame C, there is evidence of twisting of the web and inner flange near the contact region. All the

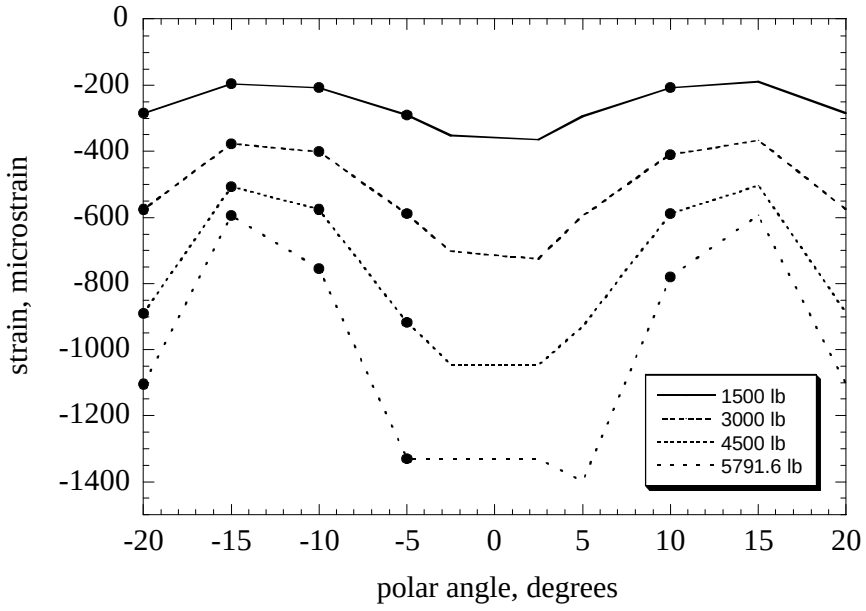

Fig. 5.6 Extensional strain data from the test of frame B.

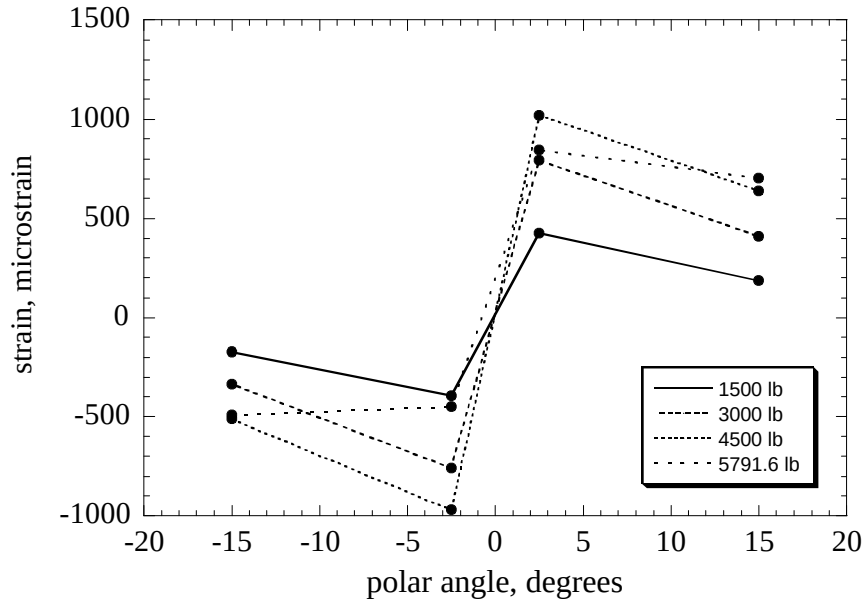

Fig. 5.7 Shear strain data in the web from the test of frame B.

strain gages show a linear response up to a displacement of about 0.12 in. (about 1760 lb). From that point on, the majority of the strain gages show a non-linear response with respect to load.

The circumferential strains from gages 16 and 17 plotted with respect to the load are shown in Fig. 5.8. These gages are located at a polar angle q = -1°, on the concave surface

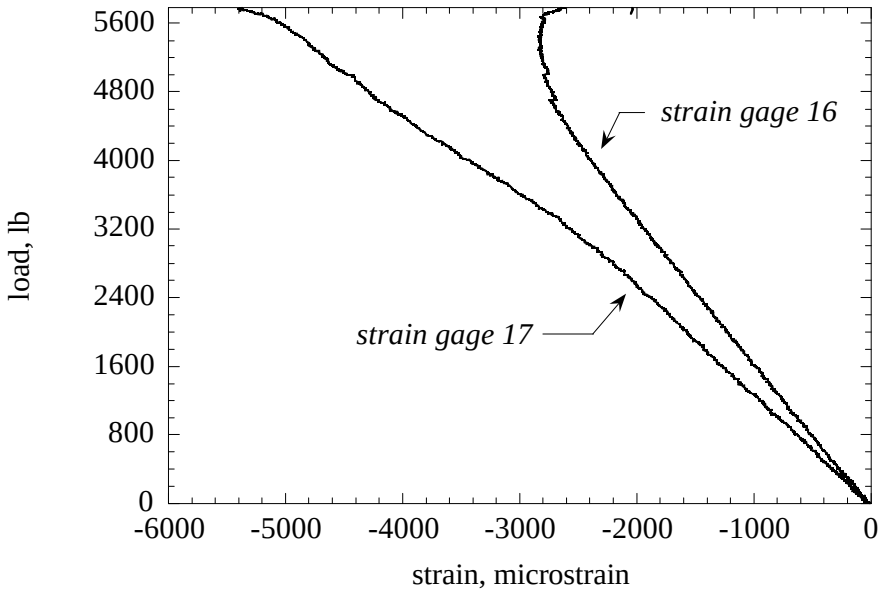

Fig. 5.8 Circumferential strains from gages 16 and 17 on the outer flange at q = -1° in the test of frame B.

of the outer flange, one in the front of the flange, one in the back (see Fig. 4.8, and Table 4.3). The fact that these gage readings are different reflects the out-of-plane bending of the frame; this difference can be noticed almost since the beginning of the test. Both gages are in compression, and gage 17 registers relatively high levels of compressive strains. At the first failure event (B_1), the difference between the readings of the gages is about 3000 με.

The circumferential strains from back-to-back gages 11 and 15, which are on the convex and concave surfaces of the outer flange at q = -2.5°, are plotted with respect to load in Fig. 5.9. Gages 11 and 15 record compressive strains of unequal value. In particular, at the first major failure event (B_1), the compressive strain magnitude of gage 11 is about

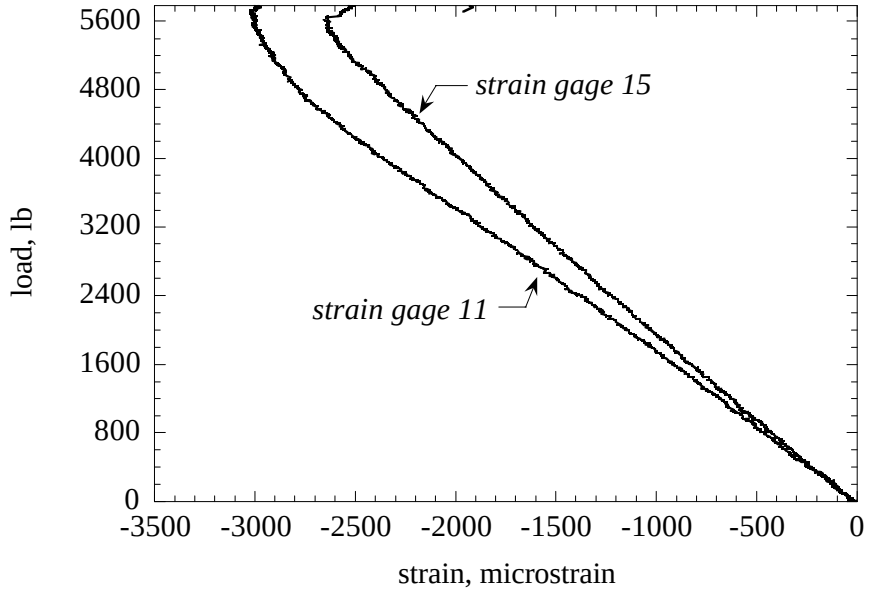

Fig. 5.9 Circumferential strains from back-to-back gages 11 and 15 on the outer flange at q = -2.5° in the test of frame B.

3000 με, which is considerably smaller than the material compressive failure strain of 10108 με predicted by TEXCAD in Table 3.14 on page 75. So, this strain data suggests local buckling of the outer flange near the point of load application.

Circumferential strains from back-to-back gages 24 and 30, which are at the convex and concave sides at the center of the inner flange at q = 0°, are shown in Fig. 5.10. At the same location of the inner flange, gages 23 and 29 record back-to-back strains in the out-of-plane direction, shown in Fig 5.11. The inner flange is in circumferential tension at q = 0°, but the differences in the back-to-back gages on the inner flange reflect local bending, or curling of this flange. The strain data suggests that cross-sectional distortion is significant near the failure load.

5.2 Test results of braided composite frame C

The load-displacement curve from the test of braided frame C, like the curve of frame B, is linear in the initial portion followed by a softening response. See Fig. 5.12. The slope

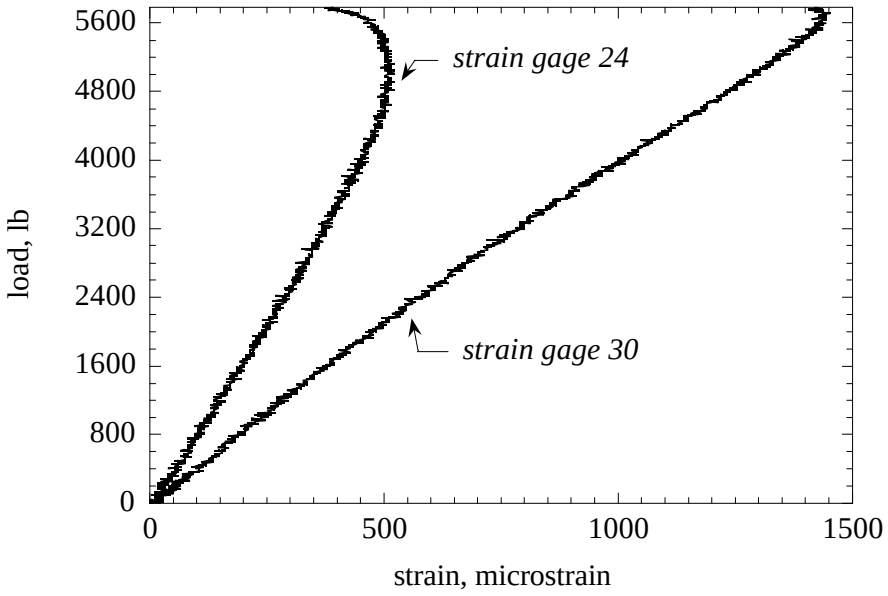

Fig. 5.10 Circumferential strains from gages 24 and 30 on the inner flange at q = 0° in the test of frame B.

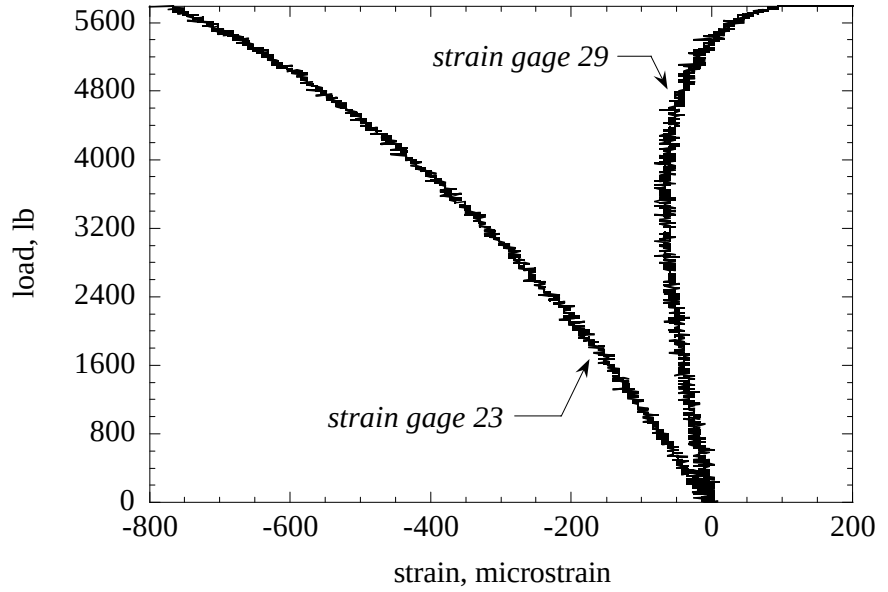

Fig. 5.11 Out-of-plane strains from gages 23 and 29 on the inner flange at q = 0° in the test of frame B.

of this linear portion is about 15590 lb/in., which is about 5% larger than for frame B, and decreases from this value to the first major failure event. At the center of the frame (q = 0°), curling of the back side of the outer flange is observed prior to the first failure. (The

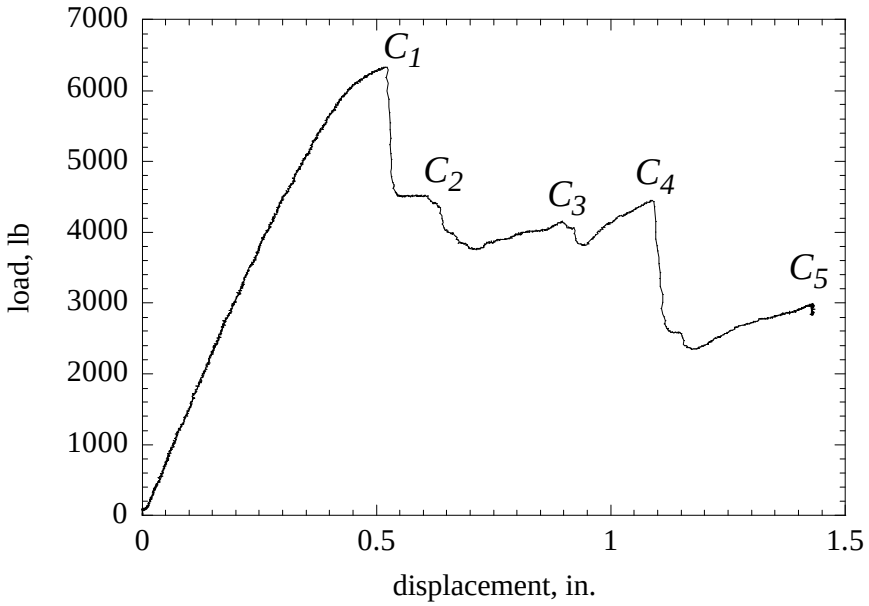

Fig. 5.12 Load-deflection curve of braided composite frame C test.

back side of the J-section refers to side opposite to the inner flange, or for the side of the web in the cross section where the *y*-coordinate is negative. Refer to Fig. 4.9 on page 88.) The first major failure event occurs at the point labeled C_1 (6331.9 lb, 0.5187 in.). This failure manifests as a crack in the back side of the outer flange at $q = 0°$, beginning at the junction of the web and outer flange. Also, damage appears to begin at $q = \pm 5°$ in the front part of the outer flange. As the test continues, the material in the web and along the junction of the web and outer flange deforms in such a manner to suggest that the crack is extending internally from the center ($q = 0°$) to $q = \pm 5°$. After the first failure, a drop in the force is observed, from 6331.9 lb to 4494.5 lb. After this first drop in the force, the force remains almost constant as the displacement increases. The second failure event begins at point C_2 (4517.9 lb, 0.601 in.), after which there is small drop in force. Then the force drops slightly again to 4416.4 lb at a displacement of 0.6293 in. This second failure event initiates at the junction of the web and outer flange at $q = -5°$ and propagates toward the front of the outer flange at this circumferential location. After this, the force drops to 4000.0 lb, and continues dropping slightly until reaching 3752.7 lb, corresponding to a displacement of 0.714 in. As the test continues, a very slight and irregular reloading is observed, until the third failure event at point C_3 (4153.5 lb, 0.8969 in.) occurs. Then the

load drops slightly to 4065.0 lb, corresponding to a displacement of 0.9196 in. In this third failure event the crack that began at q = -5° in the front side of the outer flange propagates to the back of the flange. The force drops to 3815.2 lb, and reloading initiates again to the fourth failure C_4 (4450.2 lb, 1.0847 in.). At q = -5°, the crack in the front part of the outer flange grows to completely fracture the flange and simultaneously another crack begins to propagate from the interface between the web and outer flange into the web. Also at this time, at q = -7° the back of the outer flange fractured. The force then drops to 2641.5 lb. The fifth failure event C_5 begins at 2589.4 lb and 1.1491 in. At q = -5° the inner flange is cracked. The crack in the outer flange propagates radially into the web to a length of about 2 in. and then turns in the circumferential direction increasing its length to about 3 inches. So, this fracture, located in the front side of the web is L-shaped as shown in Fig. 5.13. At

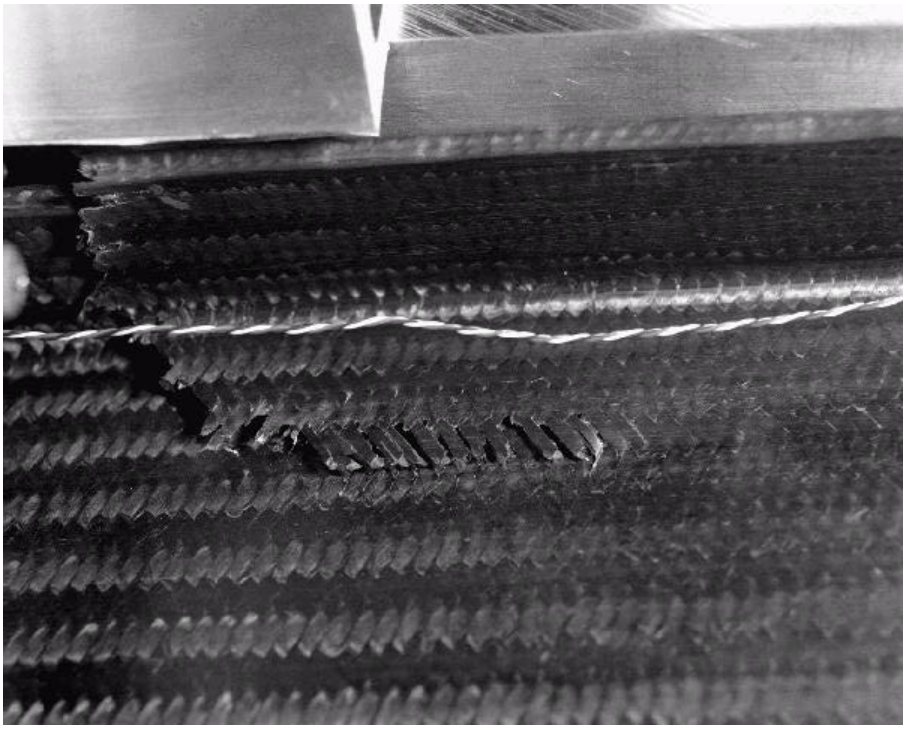

Fig. 5.13 L-shaped crack in the web of braided composite frame C at q = -5°.

q = -7°, the fracture that began in the back side of the outer flange, extends to the front.

When compared to the response of braided frame B, the failure events on frame C occur at similar displacement magnitudes as in frame B, but at different locations in both frames. Cracks develop in frame B in the outer flange and radially along the web at the apex (q = 0°), and in the inner flange at the ends (q = ± 21.4°). The cracks in frame C develop at several locations: in the outer flange at q = 0°, ± 5°, and -7°, and in the inner flange and web at q = -5°. The reason for these different failure locations could be related to defects in the composition of the braided material. There are maybe voids, resin rich zones and resin starved zones, that could influence crack initiation sites and crack paths. Further inspection of frame C after the test reveals a crack at the junction of the web and outer flange extending circumferentially from -9° to 9°. Over this same circumferential arc length, two parallel, circumferential fractures isolate a ligament of material at the center of the outer flange, with some of this material slightly protruding from the flange. See Fig. 5.14. This ligament of material appears to be a filler inserted into the surface of the outer flange just above the junction with the web.

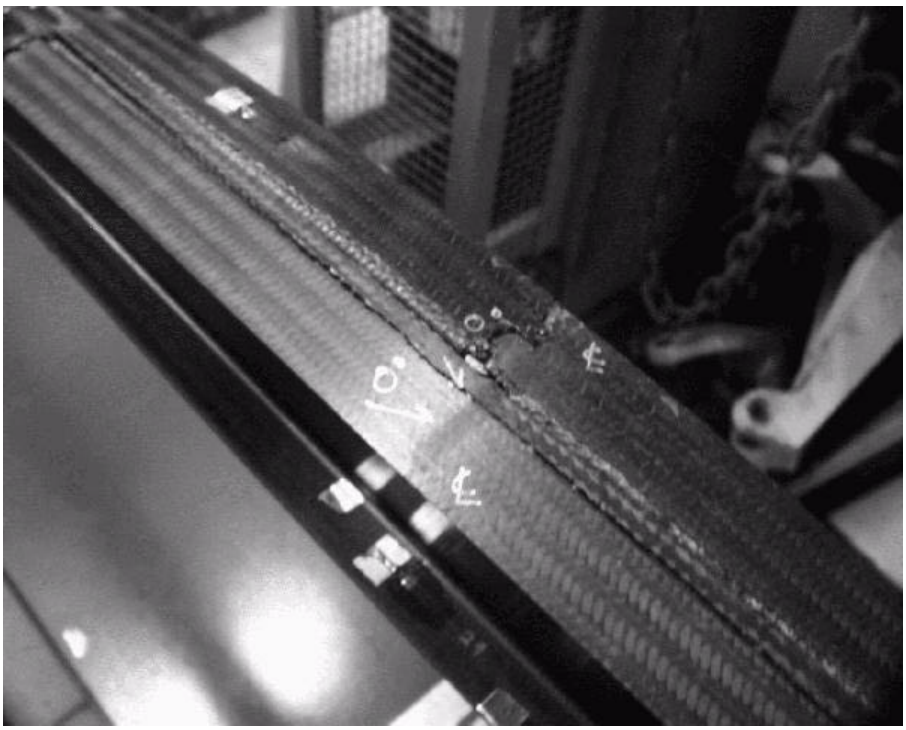

Fig. 5.14 Parallel, circumferential cracks in the outer flange over the junction with the web in frame C.

The circumferential strain distributions in the outer flange at different load levels from the test of frame C test are shown in Fig. 5.15. Like in the test of frame B, the maximum

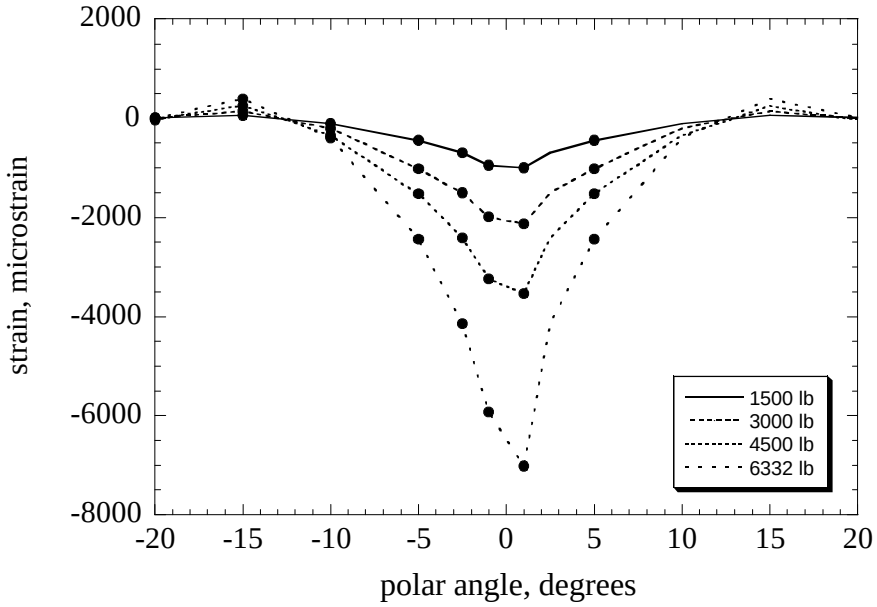

Fig. 5.15 Circumferential strain distribution in the outer flange of frame C at different load levels.

compressive strain magnitude in the outer flange occurs close to the center of the specimen ($q = 0°$), and the maximum tensile circumferential strains occur near $q = \pm 15°$. The maximum compressive strain magnitude is much larger than the maximum tensile strain magnitude for a given load level. The circumferential strain distribution on the inner flange at different load levels for frame C is shown in Fig. 5.16. In these plots there is a peak tensile strain at the center of the specimen ($q = 0°$) and maximum compressive strain magnitudes at the ends of the frame. The peak tensile circumferential strain in the inner flange is less than the maximum compressive strain magnitude at a given load level. The in-plane bending strain distribution and stretching strain distribution shown in Figs. 5.17 and 5.18, respectively, follow what is observed in frame B. Also, as in frame B, the plot of the bending strain distribution exhibits inflection points; i.e., a locations where, independent of the load level, the bending strain vanishes. These inflection points, as in frame B, appears to be located about $q = \pm 8°$ to $\pm 9°$. The shear strain distributions on the front side

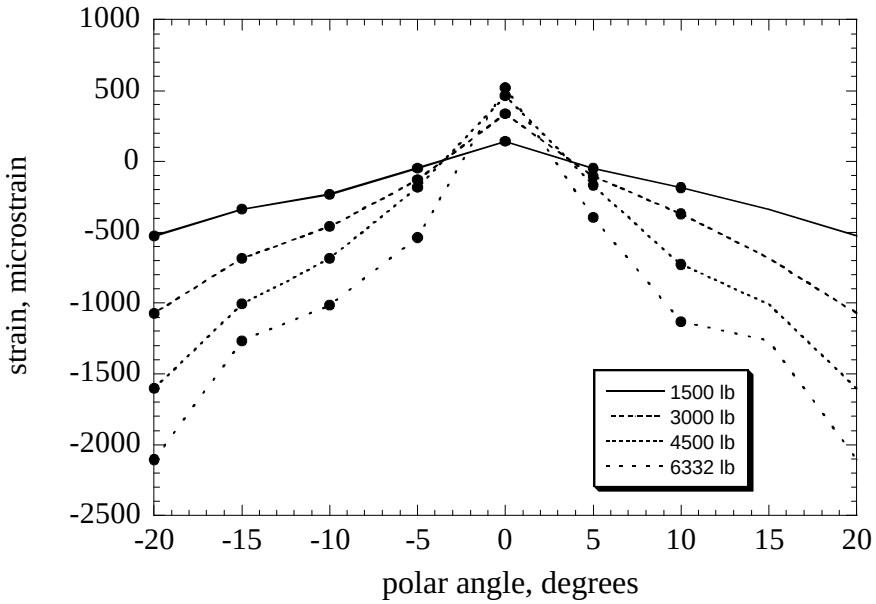

Fig. 5.16 Circumferential strain distribution in the inner flange of frame C at different low levels.

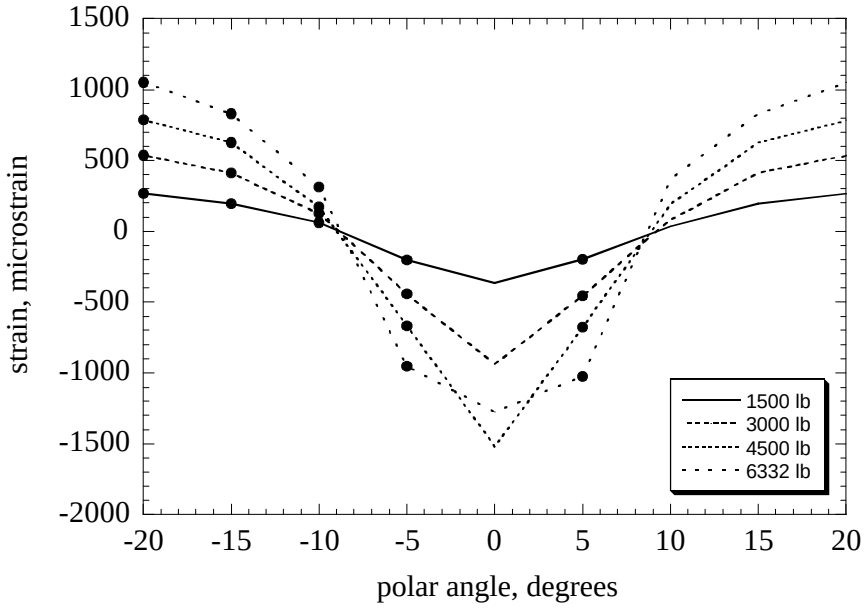

Fig. 5.17 Circumferential bending strain distribution of braided composite frame C at different load levels.

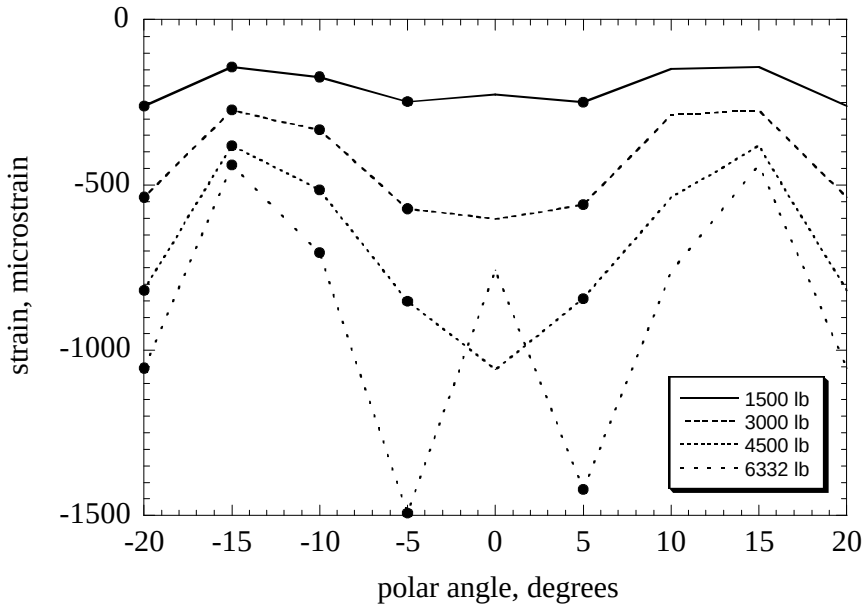

Fig. 5.18 Circumferential extensional strain distribution of braided composite frame C at different load levels.

of the web are shown in Fig. 5.19 at different load levels. These shear strain distributions follow the same shape and behavior as the plots obtained in the test of frame B

Six three-element-rosettes are located as back-to-back in pairs at $q = 5°$, in the outer flange, the web, and the inner flange, to study the twist and other shear effects at that location. The middle surface shear strain is estimated as the average of the shear strains from each back-to-back rosette pair. Plots of middle surface shear strains at $q = 5°$ as a function of the applied displacement at the apex are shown in Fig. 5.20. This middle surface shear strain is nearly zero for the outer flange; the irregular response observed after a displacement of about 0.3 in. is probably due to contact with the platen. The plots corresponding to the response in the web and in the inner flange are nonlinear. The magnitude of the middle surface shear strain in the web at failure is about 1500 με, and the magnitude of the middle surface shear strain in the inner flange at failure is about 2500 με. This distribution of the middle surface shear strain around the contour in the cross section suggests that the shear flow is largest in the inner flange.

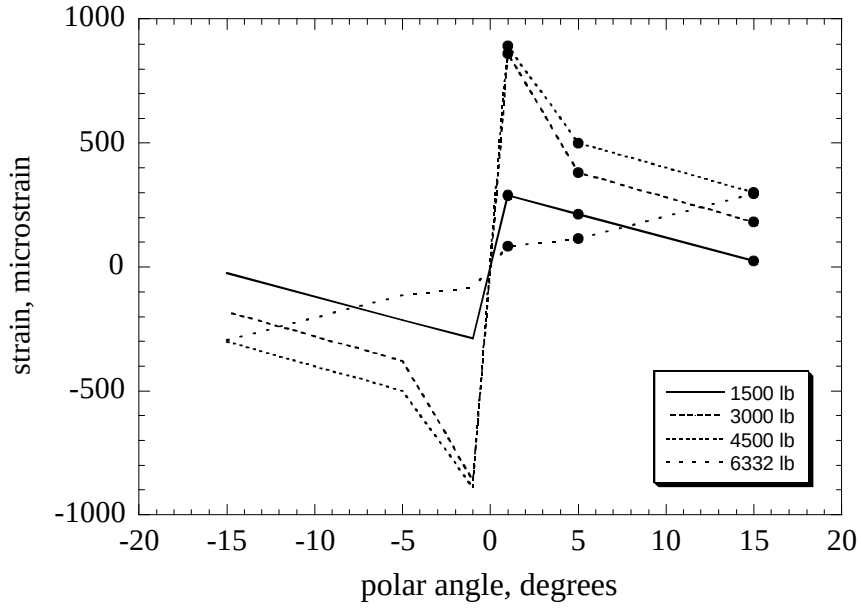

Fig. 5.19 Shear strain distribution on the back of the web of frame C at different load levels.

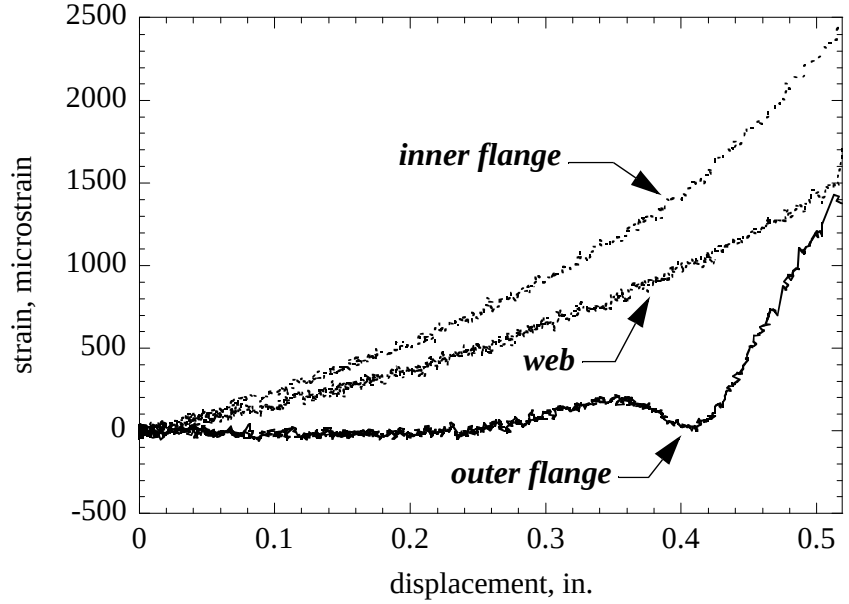

Fig. 5.20 Middle surface shear strain distribution in the cross-section at q = 5° of frame C.

In thin-walled, open section bar theory one-half the difference in the shear strains from back-to-back strain gages is attributable to the twist of the section in torsion. So we define one-half the difference in the surface shear stains from back-to-back gages as the shear strain due to twist. Plots of the shear strain due twist in the cross-sectional elements at q = 5° as a function of the applied displacement at the apex are shown in Fig. 5.21. The shear strain in twist is small in the inner flange, and largest in the web. Hence, these shear strain distributions in the cross section suggest that the web and outer flange carry most of the torque, or twisting moment.

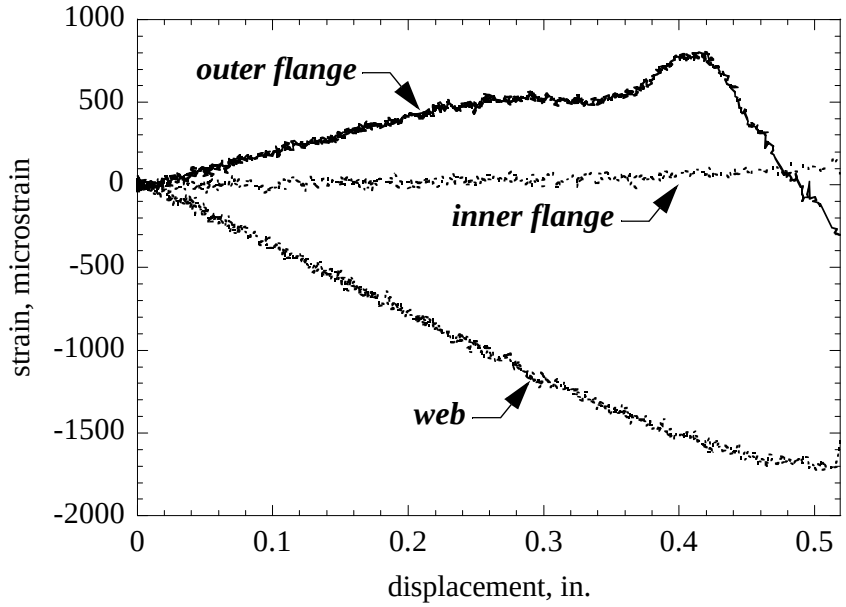

Fig. 5.21 Shear strains due to twist in the cross-section at q = 5° from frame C.

Two LVDTs are mounted to contact the center of the web at q = 0°, and q = -5° of frame C in order to measure the out-of-plane displacements (V) at these locations. The displacements measured by these LVDTs are shown in Fig. 5.22. In addition, an inclinometer is located at q = -12.5°, close to the center of the outer flange, to measure the twist (F_x). The measured twist at q = -12.5° as a function of the applied displacement at the apex of the frame is shown in Fig. 5.23. The plots of the out-of-plane displacements from the LVDTs are nonlinear, particularly for the displacement from LVDT located at q = 0°. The

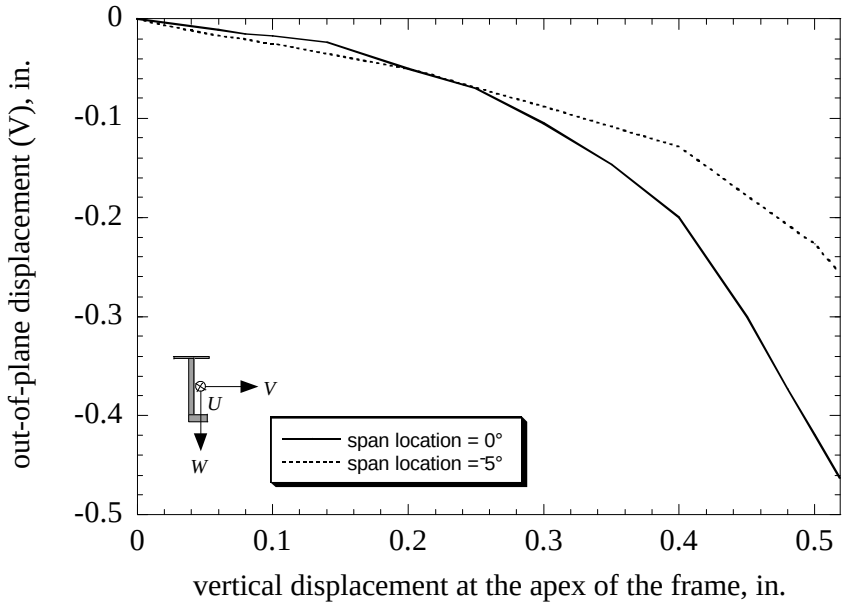

Fig. 5.22 Out-of-plane displacement at two different locations on frame C.

displacement of the LVDT located at q = 0° is about 0.46 in. when the frame failed; the LVDT located at q = -5° records a displacement of about 0.3 in. at failure. The response plot of the inclinometer is also nonlinear. This instrument records a rotation of about 3° at failure.

5.3 Analytical model using the computer code ABAQUS

Models of frames B and C using version 5.8-1 of the computer code ABAQUS are developed to analyze the test results. The frame is modeled as a series 24 thin-walled curved beam elements, denoted in the code as B32OS. These quadratic beam elements have seven degrees of freedom at each node: three displacements, three rotations, and warping of the cross-section. They use Timoshenko beam theory, and include transverse shear deformation. The end conditions are clamped, except for the warping that is unrestrained. The analysis is linear elastic, and a progressive failure model of the textile composite material is not included. The stiffness matrix is required as input to the ABAQUS code. The matrix used is the wall stiffness matrix (elasticity matrix) of the $[0°_{18k}/\pm 64°_{6k}]$ 39.7 % axial braided composite material obtained from TEXCAD. There is no extension-shear coupling in the effective elastic properties of the braided layer, and each branch of the cross

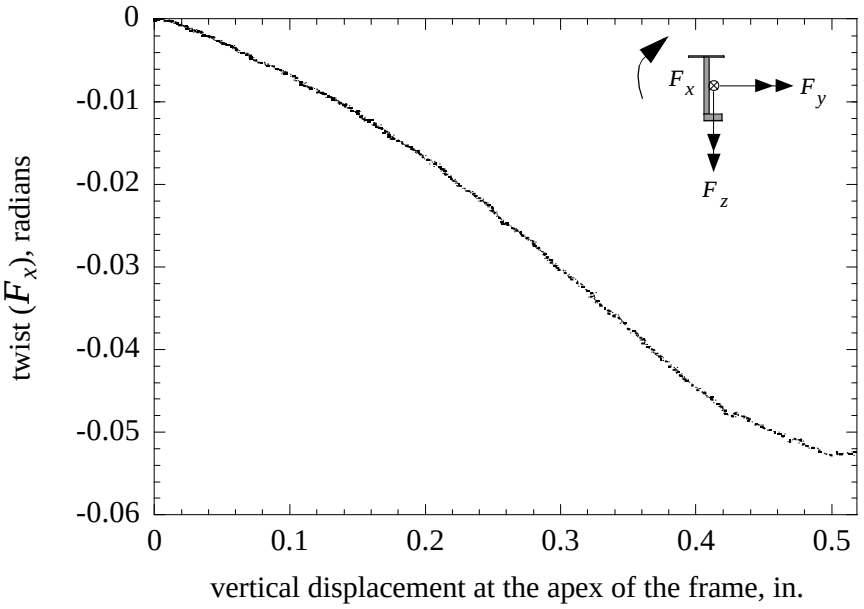

Fig. 5.23 Twist of the outer flange of frame C at q = -12.5°.

section (web and flanges) is assumed to have the same elastic properties. The load-displacement curves from the ABAQUS analysis and the test results are plotted in Fig. 5.24 The load predicted by the analysis corresponding to the displacement of the test of frame B at failure, 0.4782 in., is 7162 lb. The load predicted by the analysis corresponding to the displacement of the test of frame C at failure, 0.5187 in., is 8289 lb. The ABAQUS model predicts the stiffness of the frames in the tests relatively well. The slope of the load-displacement plot predicted by the analysis for frame B is 14,977 lb/in., which is less than 1% larger than the stiffness of 14,887 lb/in. obtained from the test. The stiffness predicted for frame C is 15,980 lb/in., which is less than 3% larger than the stiffness of 15,590 lb/in. obtained in the test..

The distributions of the displacements along the circumference predicted by the ABAQUS analysis for frame B are plotted in Fig. 5.25. The displacement curves look qualitatively correct based on observations made during the tests of frames B and C. One of the most peculiar theoretical responses that these plots show is the large value of the out-of-plane displacement (V). The out-of-plane displacement obtained from the analysis is comparable in magnitude to the value of the applied, radially inward displacement (W)

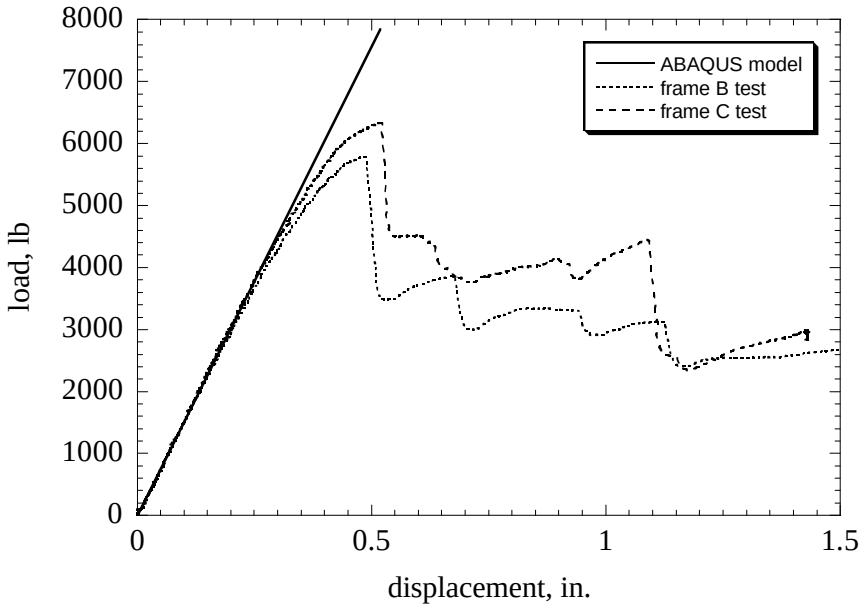

Fig. 5.24 Load-displacement response from the ABAQUS analysis and from the tests of frames B and C.

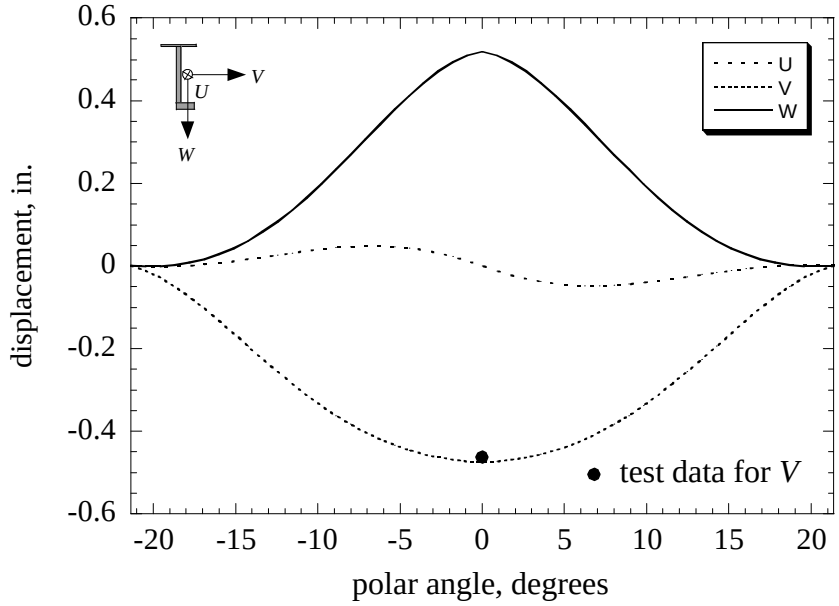

Fig. 5.25 Displacement distributions of frame C from ABAQUS at the first failure event.

at the apex. This out-of plane displacement is negative, indicating a motion backward, or in the negative y-direction (see Fig. 4.9 on page 88). The magnitude of the out-of-plane

displacement at q = 0° obtained from the test of frame C at failure is 0.46 in., which compares very well with the predicted magnitude of 0.48 in.

The distributions of the rotations along the circumference predicted by the ABAQUS analysis of frame B are plotted in Figs. 5.26. The rotation about the circumferential axis,

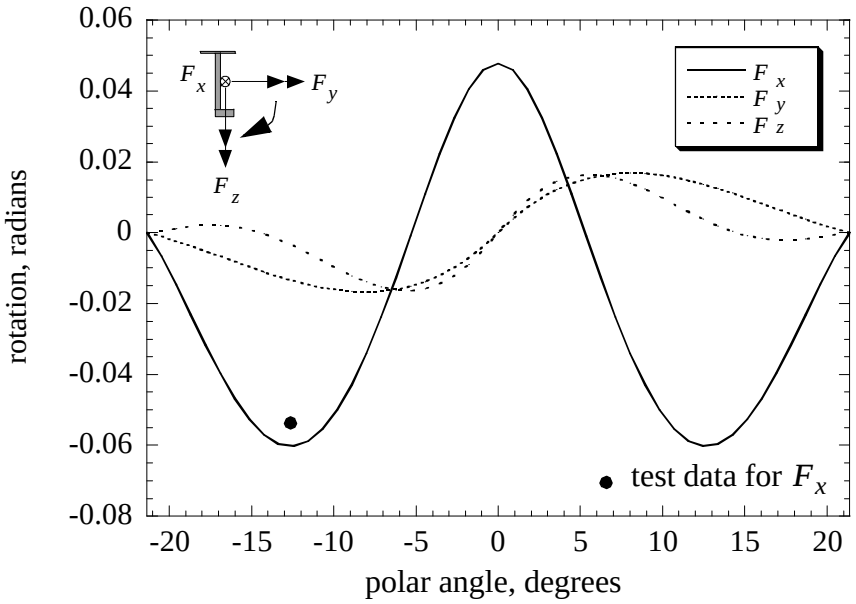

Fig. 5.26 Distribution of the rotations of frame C from ABAQUS at the first failure event.

or twist, of the frame (F_x) predicted by the analysis is relatively large. According to the ABAQUS model, the magnitude of the twist is higher at the center of the frame (q = 0°), and at approximately q = ± 12.5°. This distribution of the twist is in qualitative agreement with the observations made during the test. The frame twists from the beginning of the test, and it is noticed that the center of the frame moves in the negative y-direction at the moment of failure. The magnitude of the twist measured at q = -12.5° is about 0.053 radians at failure, which is comparable in magnitude to 0.060 radians predicted from the analysis.

The circumferential strain distribution at the four load levels of 1500 lb, 3000 lb, 4500 lb, and 5791.6 lb for frame B are plotted in Figs. 5.27-5.30, respectively. Failure of frame

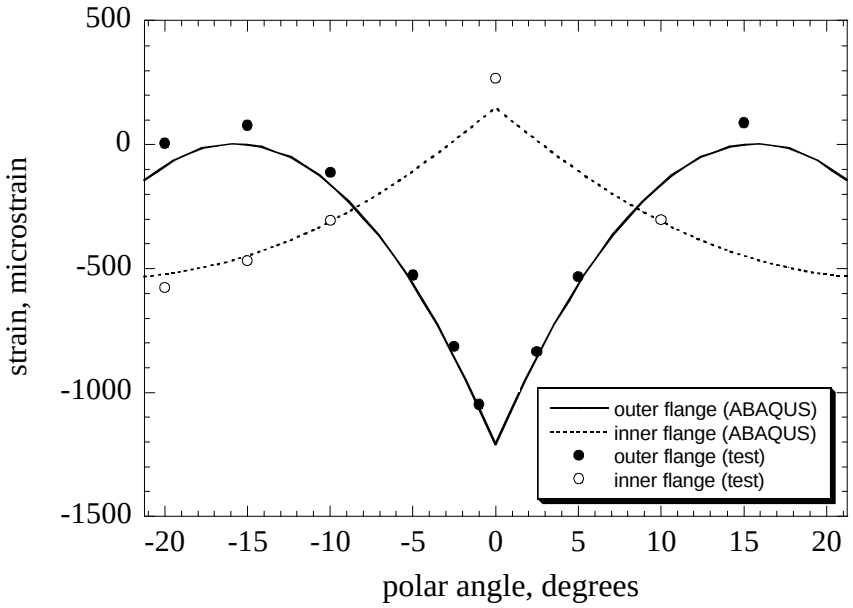

Fig. 5.27 Circumferential strain distribution at 1500 lb for frame B from ABAQUS.

B in the test occurs at 5791.6 lb and 0.4782 in. The similarities in the circumferential strain distribution plots between analysis and test results are impressive, considering the simplicity of the ABAQUS model. The shapes of the curves are very similar. In these plots, the locations where the analytical predictions are not as good are near the ends of the outer flange, and near the center of the inner flange. These are locations of low strain magnitudes. The reason for these discrepancies, at least in the case of the outer flange, can be related to the fact that in these locations the strains are measured on one external surface of the flange. The ABAQUS model calculates the strain mid-surface of the flange. Without back-to-back strain gage measurements, the mid surface strain cannot be estimated.

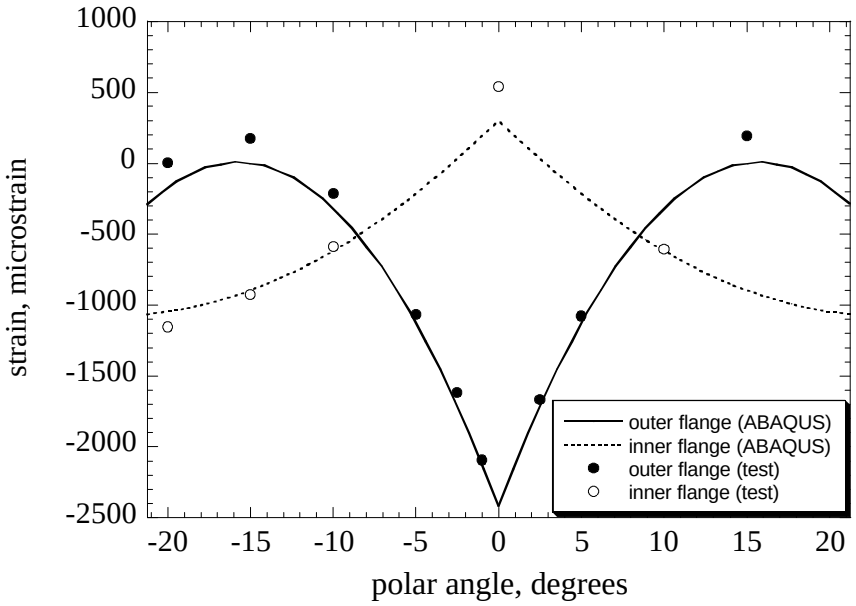

Fig. 5.28 Circumferential strain distribution at 3000 lb for frame B from ABAQUS.

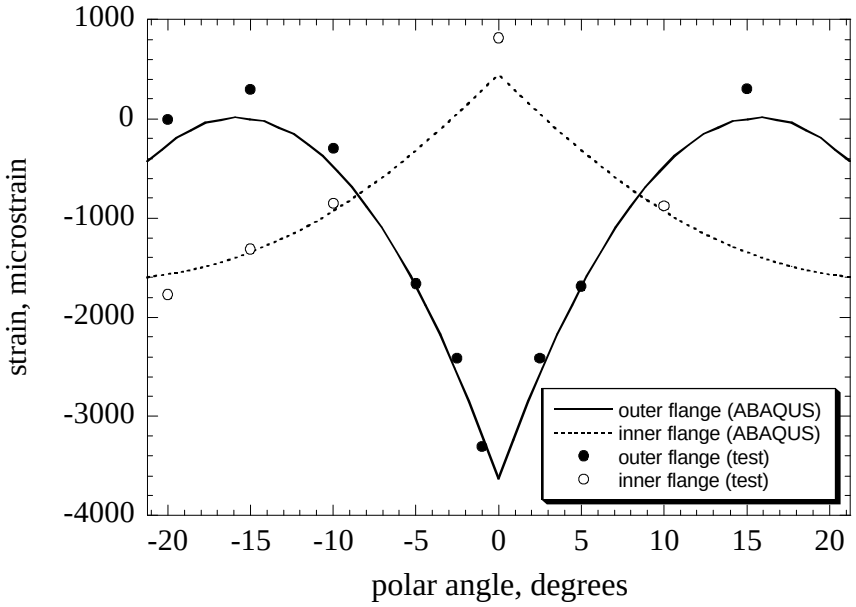

Fig. 5.29 Circumferential strain distribution at 4500 lb for frame B from ABAQUS.

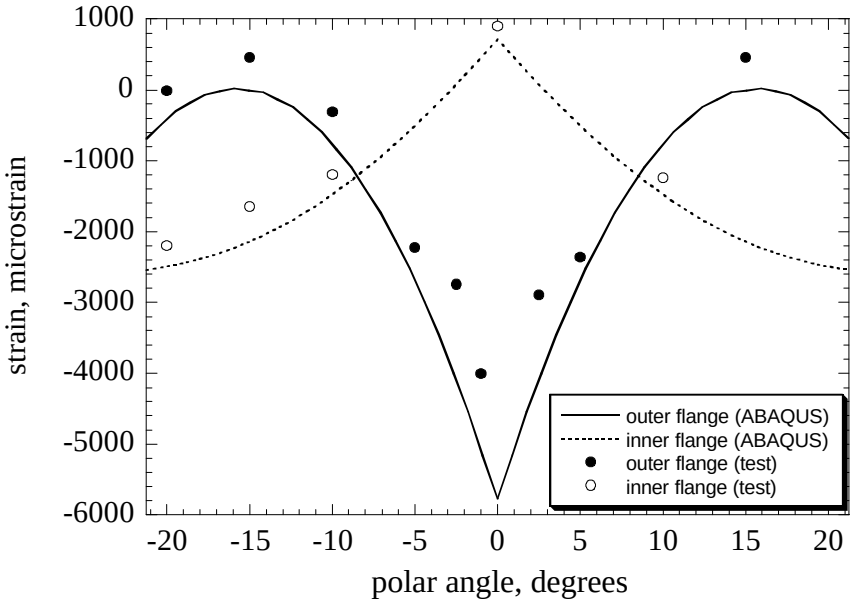

Fig. 5.30 Circumferential strain distribution at 5791.6 lb (first failure event) for frame B from ABAQUS.